ice can be seen aligned at the corners of an inner square. Fig. 2*b* shows the parallel polarisation image ($I_{||}$) of the target (the polariser in front of the CCD is parallel with the polarisation of the illuminating light) while Fig. 2*c* shows the perpendicular image component ($I_{\perp}$). As discussed above, ice depolarises light much more than metal. As a result, the ice in the parallel image appears darker than the metal, while in the perpendicular image the ice appears brighter than the metal. Fig. 2*d* shows the image obtained after subtraction of the two images' components $[I_{||} - I_{\perp}]$. The image in Fig. 2*e* was obtained by performing the $[(I_{||} - I_{\perp})/I_{\perp}]$ image operation (division over the perpendicular image after subtraction). In the resulting images shown in Fig. 2*d* and *e*, the ice is recorded with much less intensity than the metal. This demonstrates the usefulness of this technique for ice detection and imaging. The image operation $(I_{||} - I_{\perp})$ leads to an image formed by polarised photons. Since metal depolarises light much less than ice, the clear metal surface in the polarisation difference image appears much brighter compared to ice. This approach provides a means for imaging and detection of the parts of the metal surface containing ice layers. The $I_{||} - I_{\perp}$ operation allows for the rejection of the image information arising from unpolarised background illumination from sunlight or field lighting which is evenly distributed in both image polarisation components and cancelled out after subtraction.

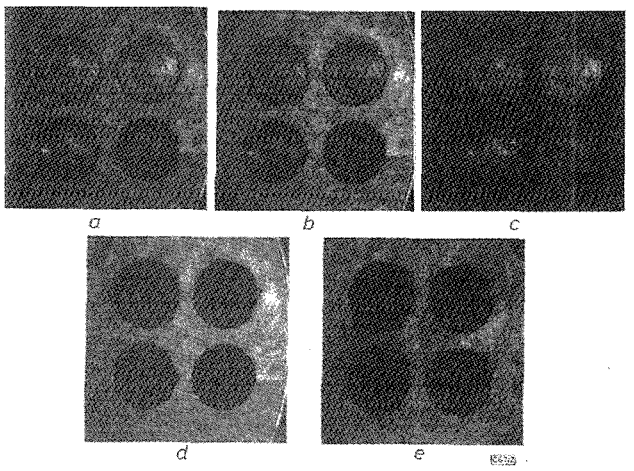

Fig. 2 *Imaging of ice on metal*

a Image of target with no polariser in front of CCD
b Parallel polarisation image ($I_{||}$) of target (polariser in front of CCD is parallel with polarisation of illuminating light)
c Perpendicular image component ($I_{\perp}$)
d Image obtained after subtraction of two images components $[I_{||} - I_{\perp}]$
e the $[(I_{||} - I_{\perp})/I_{\perp}]$ image (division over the perpendicular image after subtraction)

Detection of ice can be performed by either scanning or flooding the wing of an airplane with a polarised light beam and detecting point-by-point the depolarisation of the reflected light. The intensities of the two polarisation components of the initially polarised beam are simultaneously measured and the ratio of the parallel over the perpendicularintensities from each point on the wing$(I_{||}/I_{\perp})$ is estimated. From the image shown in Fig. 2, the ratio $R = I_{||}/I_{\perp}$ was measured to be $R_{met} \simeq 40$ for the clear metal part and $R_{0.25mm} \simeq 2.25$, $R_{0.5mm} \simeq 1.4$, $R_{1mm} \simeq 1.25$, and $R_{2mm} \simeq 1.2$ for the ice layers on metal with thickness 0, 0.25, 0.5, 1 and 2mm, respectively. These results indicate that when the ratio is high $[(I_{||}/I_{\perp}) \gg 1]$, then the wing is free of ice in accordance with results shown in Fig. 1*a*. When the ratio becomes nearly 1 $(1 < (I_{||}/I_{\perp}) < 3)$ there is ice on this part of the wing.

This work demonstrates the potential for an ice detection imaging system for aviation applications.

Acknowledgments: This research is supported by the New York State Science and Technology Foundation.

14 October 1996
Electronics Letters Online No: 19961532

S.G. Demos and R.R. Alfano (*Institute for Ultrafast Spectroscopy and Laser, New York State Center for Advanced Technology for Ultrafast Photonic Materials and Applications, Department of Physics, The City College and Graduate School of the City University of New York, New York, NY 10031, USA*)

References

1 GIBBS, D.P., BETTY, C.L., BREDOW, J.W., and FUNG, A.K.: 'Polarised and cross-polarised angular reflectance characteristics of saline ice and snow', *Remote Sens. Reviews*, 1993, **7**, pp. 179–195
2 RENAU, J., CHEO, P.K., and COOPER, H.G.: 'Depolarization of linearly polarised EM waves backscattered from rough metals and inhomogeneous dielectrics', *J. Opt. Soc. Am.*, 1967, **57**, (4), pp. 459–466
3 ULABY, F.T., MOORE, R.K., and FUNG, A.K.: 'Microwave remote sensing, Vol. III' (Artech House, Inc., Norwood, 1986), pp. 1826–1827
4 JAKOBY, R., RÜCKER, F., VANHOENACKER, D., and VASSEUR, H.: 'Fraction of ice depolarisation on satellite links in Ka band', *Electron. Lett.*, 1994, **30**, (23), pp. 1917–1918

Fuzzy modelling using wavelet transforms

Chuan-Kai Lin and Sheng-De Wang

Indexing terms: Neural networks, Fuzzy neural nets, Wavelet transforms

A new approach to fuzzy modelling using wavelet transforms is proposed. A fuzzy inference system with some minor restrictions and modifications can function as a discrete wavelet transform. The feasibility of the proposed fuzzy model is proved by modelling a highly nonlinear function and comparing it with previous research.

Introduction: Control engineers always face the problems of modelling systems that could be so complex and nonlinear as very difficult to obtain. Fuzzy models have provided a good solution to overcome this problem. However, fuzzy systems require formal synthesis techniques that guarantee global stability and acceptable performance [1]. In this Letter, we show that fuzzy models, with some restrictions and modifications, can be functionally equivalent to discrete wavelet transforms. Therefore, the fuzzy models can take advantage of the rigorous approximation theory of wavelet basis function expansions as well as offer a framework for combining linguistic information and numerical data in a unified fashion.

Discrete wavelet transforms: Given a function $\psi \in L^2(R^n)$, consider the sequence functions $\{\psi_{j,k}\}$ generated by dilating and translating the mother wavelet function ψ into the following form:

$$\psi_{j,k}(x) = \det D_j^{1/2} \psi(D_j x - \Lambda_k k) \qquad (1)$$

where $j = [j_1, \ldots j_n]^T \in Z^n$, $k \in Z^n$, the dilation matrix $D_j = \mathrm{diag}(a^{j_1}, \ldots, a^{j_n})$, the translation matrix $\Lambda_k = \mathrm{diag}(b_1, \ldots, b_n)$, $a > 1$, $a \in R$, $b = (b_1, \ldots, b_n) \in R^n$. Conditions on ψ, a and b to form a multiscaling wavelet frame for $L^2(R^n)$ have been obtained and are given in [4]. Then, consider a class of multidimensional wavelet functions as generalisations of 1D wavelet functions [4], i.e.

$$\psi(x) = \psi_1(x_1) \cdots \psi_n(x_n) \qquad (2)$$

The sequence functions $\{\psi_{j,k}\}$ are a set of wavelet basis functions to constitute a frame for a class of functions $f \in L^2(R^n)$ to be approximated. Therefore, f can be reconstructed by the expansion of $\{\psi_{j,k}\}$ exactly [3]. In this Letter, the mother wavelets have the form

$$\psi_i(x_i) = g_i(x_i) e^{-\alpha_i x_i^2/2} \qquad (3)$$

satisfying $\int \psi_i(x_i) dx_i = 0$. For example, the 'Mexican Hat' mother wavelet function is

$$\psi_i(x_i) = \alpha_i (1 - \alpha_i x_i^2) e^{-\alpha_i x_i^2/2}$$

Substituting the 'Mexican Hat' mother wavelet function into eqns. 1 and 2 yields

$$\psi_{j,k} = a^{-j_1/2}\alpha_1[1-\alpha_1(a^{-j_1}x_1-b_1k_1)^2]e^{-\alpha_1(a^{-j_1}x_1-b_1k_1)^2/2}\ldots a^{-j_n/2}\alpha_n[1-\alpha_n(a^{-j_n}x_n-b_nk_n)^2]e^{-\alpha_n(a^{-j_n}x_n-b_nk_n)^2/2} \quad (4)$$

Eqn. 4 illustrates a way to constitute a set of wavelet basis functions with multiresolution to form a multiscaling frame.

Functional equivalence between wavelet transforms and fuzzy models: The rule format of the proposed fuzzy model can be written as follows:

$$\text{Rule } m: \text{ if } x \text{ is } \tilde{A}_{m1} \text{ and } \ldots \text{ and } x_n \text{ is } \tilde{A}_{mn} \text{ then } y_j = d_m g_{m,1}(x_1)\cdots g_{m,n}(x_n) \quad (5)$$

where $\tilde{A}_{m1}$, $\tilde{A}_{m2}$, ... and $\tilde{A}_{mn}$ are fuzzy sets with Gaussian membership functions, $g_{m,l}(x_l)$ are functions shifting and scaling $g_l(x_l)$, and d_m are real coefficients. By applying the min-product inference process, the output y_j is

$$y_j = \frac{\sum_m \left[d_m \prod_{l=1}^{n} \mu_{\tilde{A}_{ml}}(x_l) g_{m,l}(x_l)\right]}{\sum_m \prod_{l=1}^{n} \mu_{\tilde{A}_{ml}}(x_l)} \quad (6)$$

where index $j = [j_1, \ldots j_n]^T$, and $\mu_{\tilde{A}_{ml}}(x_l)$ is the membership function of $\tilde{A}_{ml}$. The fuzzy rule base is implemented by multiple fuzzy rule bases corresponding to the multiresolution wavelet functions. The output y_j is the output of fuzzy rule base j corresponding to a resolution. Assume the centres of membership functions of linguistic terms are equally spaced. For a given resolution j, the centres of fuzzy basis functions are located in lattice points in R^n. Denoting a sequence of basis vectors for the lattice as $\{\vec{e}_1, \ldots \vec{e}_n\}$, and the lattice points can be represented by

$$\eta_k = k_1 a^{j_1} b_1 \vec{e}_1 + \cdots + k_n a^{j_n} b_n \vec{e}_n \quad (7)$$

where $a^{j_i}b_i$ is the sampling space in ith dimension. From the geometric point of view, each lattice point is a fuzzy basis function $\phi_{j,k}$:

$$\phi_{j,k} = \frac{e^{-(x-\eta_k)^T W_j (x-\eta_k)}}{\sum_{k\in Z^n} e^{-(x-\eta_k)^T W_j (x-\eta_k)}} \quad (8)$$

where $W_j = \text{diag}\{\alpha_1/(a^{j_1})^2, \ldots, \alpha_n / (a^{j_n})^2\}$. Hence, the output of each fuzzy rule base is of the form

$$y_j = \sum_k d_{j,k}\psi_{j,k} \quad (9)$$

where $\psi_{j,k} = g_{j,k,1}(x_1) \ldots g_{j,k,n}(x_n)\phi_{j,k}$ and $d_{j,k}$ are real coefficients. Take eqn. 4 as an illustration, $g_{j,k,i}(x_i) = a^{j_i/2}\alpha_i[1-\alpha_i a^{-j_i}x_i - b_i k_i)^2]$. Applying the proposed fuzzy model to approximate function f is as follows:

$$f = \sum_j y_j = \sum_j \sum_k d_{j,k}\psi_{j,k} \quad (10)$$

Therefore, it is easy to show the equivalent functional behaviour of the multiresolution wavelet transform and the proposed fuzzy model.

There are various update laws for tuning coefficients of eqn. 10, such as LMS, Kalman filter algorithms, and the back-propagation law. The fuzzy model may consist of two parts: one is rules extracted from experts and the other is the rules learned from numerical data as described above.

Simulation: The highly nonlinear function modelled and predicted in our simulation is the chaotic Mackey-Glass equation:

$$\dot{x}(t) = \frac{0.2x(t-\tau)}{1+x^{10}(t-\tau)} - 0.1x(t) \quad (x(0)=1.2,\ \tau=17) \quad (11)$$

The 500 training and 500 checking data are in the following form:

$$[x(t-18)x(t-12)x(t-6)x(t)]|x(t+6)]$$

We only use a single fuzzy rule base (single resolution) in this example. The output of the optimal fuzzy rule base, $f^* = \Sigma_k d_k^* \psi_k$, is estimated by the actual fuzzy output $y = \Sigma_k \hat{d}_k \psi_k$ and disturbance rejection signal $\hat{w}$. That is, we use $\hat{f} = \Sigma_k \hat{d}_k \psi_k + \hat{w}$ to model and predict $x(t+6)$. The update laws are

$$\dot{\hat{d}}_k = k_d e \psi_k \quad \text{and} \quad \dot{\hat{w}} = k_w e \quad (12)$$

where k_d and k_w are constant and $e = x(t+6) - f$. Eqn. 12 can prove that the time derivative of $V = 1/2(e^2 + \Sigma_k \tilde{d}_k^2 + \tilde{w}^2)$ is negative or zero ($\tilde{d}_k = d_k^* - \hat{d}_k$ and $\tilde{w} = w^* - \hat{w}$). Table 1 lists the generalisation capability of the proposed model after 500 epoch learning compared with previous research [5]. The performance index NDEI is defined as the root mean square error divided by the standard deviation of the checking data. The proposed fuzzy model uses 81 rules and 81 adjustable parameters because the number of membership functions assigned to each input is three and α_i and $a^{j_i}b_i$ are set 4.5 and 0.45 for i = 1, 2, 3, 4, respectively. This example has demonstrated the effectiveness of the proposed fuzzy model.

Table 1: Generalisation capability comparisons

Method	Training cases	NDEI
Proposed fuzzy model	500	0.017
Back-propagation NN	500	0.02
Six-order polynomial	500	0.04
Cascaded-correlation NN	500	0.06
Linear predictive	2000	0.55

Last four rows are from [5]

Conclusions: This Letter presents a fuzzy model that can function equivalently to discrete wavelet transforms. Furthermore, the pivotal concept of multiple fuzzy rule bases derived from multiresolution wavelets improves the approximation accuracy. From the simulation result, the proposed fuzzy model can be applied to the problems of function approximation, system identification and control.

30 September 1996
Electronics Letters Online No: 19961508

Chuan-Kai Lin and Sheng-De Wang (*EE Building, Room 441, Department of Electrical Engineering, National Taiwan University, 1 Roosevelt Rd., Sec. 4, Taipei 106, Taiwan, Republic of China*)

E-mail: sdwang@star.ee.ntu.edu.tw

References

1 WANG, L.X.: 'Stable adaptive fuzzy control of nonlinear systems', *IEEE Trans. Fuzzy Syst.*, 1993, **1**, (2), pp. 146–155
2 BAKSHI, B.R., and STEPHANOPOULOS, G.: 'Wave-net: A multiresolution, hierarchical neural network with localised learning', *AICHE J.*, 1993, **39**, pp. 57–81
3 PATI, Y.C., and KRISHNAPRASAD, P.S.: 'Analysis and synthesis of feedforward neural networks using discrete affine wavelet transformations', *IEEE Trans. Neural Networks*, 1993, **4**, pp. 73–85
4 KUGARAJAH, T., and QINGHUA ZHANG: 'Multidimensional wavelet frames', *IEEE Trans. Neural Netw.*, 1995, **6**, (6), pp. 1552–1556
5 CROWER, R.S.: 'Predicting the Mackey-Glass time series with cascaded-correlation learning', *in* TOURETZKY, D., HINTON, G., and SEJNOVSKI, T. (Eds.): Proc. 1990 Connectionist Models Summer School, Carnegie Mellon University, 1990, pp. 117–123

100Gbit/s optical signal eye-diagram measurement with optical sampling using organic nonlinear optical crystal

H. Takara, S. Kawanishi, A. Yokoo, S. Tomaru, T. Kitoh and M. Saruwatari

Indexing terms: Optical communication, Nonlinear optics

The eye diagram of a 100Gbit/s optical signal has been successfully measured using sum-frequency-generation optical sampling, which uses an organic crystal (AANP: 2-adamantylamino-5-nitropyridine) with high optical nonlinearity to improve the signal-to-noise ratio of the measured waveform. Using this method, a signal-to-noise ratio > 17dB is obtained at a signal peak power of 270mW.